13.56 MHz High Density DC–DC Converter With PCB Inductors

Wei Liang, *Student Member, IEEE*, John Glaser, *Senior Member, IEEE*, and Juan Rivas, *Member, IEEE*

***Abstract*—This paper presents the design and implementation of a high density 150–200 V to 28 V, 200–400 W resonant dc–dc converter with embedded inductors. The converter has a switching frequency of 13.56 MHz and uses air-core toroidal inductors fabricated with printed circuit board (PCB) technology. Implementing toroidal inductors with the PCB reduces inductance variation. Hence, the tuning and implementation of the converter are simplified while achieving high levels of performance and power density. By not using magnetic cores, the inductors also maintain stable values over a wide temperature range. Moreover, the paper discusses the tradeoffs between simplicity and performance of implementing a hard-switched gate drive at megahertz switching frequencies. We describe the advantages of resonant power converter topologies in applications requiring high density and high performance in demanding environmental conditions.**

***Index Terms*—Class EF, class Φ, hard-switched gate drive, high-density dc–dc converter, printed circuit board (PCB) inductors.**

I. Introduction

THE demand for higher power density converters is on the rise and driven by the quest for more portable devices, lighter and more fuel-efficient vehicles, etc. Recent work on resonant converters has pushed switching frequency into the tens and even hundreds of megahertz while maintaining good efficiency. This reduces the energy storage requirements and leads to improvements of miniaturization [1], [2]. Among current high-frequency resonant converters, the class Φ_2 converter can reduce switch voltage stress by 30–40% below conventional class E derived converters [3]–[8] and maintain high efficiency. However, Φ_2 converter implementations suitable for operation in the hundred voltage range and up use discrete components and suffer from issues common to similar resonant topologies: 1) design tuning is time consuming as it involves iterative simulations; 2) design is sensitive to parasitics and nonlinear variations of components; and 3) gate drive design is challenging.

This paper presents a Φ_2 dc–dc converter and gate drive design addressing these issues and demonstrates experimentally a dc–dc converter with PCB inductors. This paper is organized as follows. Section II explains the circuit design. Section III details the fabrication and characteristics of air-core toroidal printed circuit board (PCB) inductors. The design of a hard-switched gate drive switching at megahertz frequencies is outlined in Section IV. Further details of the prototype and experimental results are shown in Section V. Section VI concludes this paper.

Manuscript received May 31, 2014; revised August 8, 2014; accepted August 17, 2014. Date of publication September 12, 2014; date of current version March 5, 2015. This work was supported by the Automotive Research Center and U.S. Army Tank Automotive Research, Development and Engineering Center under Cooperative Agreement W56HZV-04-2-0001. This paper was presented at the 28th Annual IEEE Applied Power Electronics Conference and Exposition, Long Beach, CA, USA, 2013. Recommended for publication by Associate Editor C. R. Sullivan.

W. Liang and J. Rivas were with the University of Michigan, Ann Arbor, MI 48105 USA. They are now with Stanford University, Stanford, CA 94105 USA (e-mail: liangw@stanford.edu, jmrivas@stanford.edu).

J. Glaser is with Efficient Power Conversion Corporation, Albany, NY 12309 USA (e-mail: john.glaser@epc-co.com).

Color versions of one or more of the figures in this paper are available online at http://ieeexplore.ieee.org.

Digital Object Identifier 10.1109/TPEL.2014.2357398

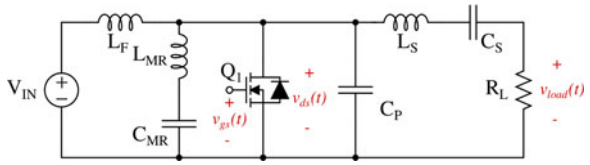

Fig. 1. Class Φ_2 inverter.

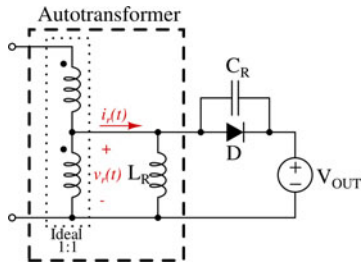

Fig. 2. Resonant rectifier with an autotransformer. When properly tuned, the fundamental component of the voltage v_r and the current i_r are in phase. The autotransformer's magnetizing inductance is labeled as L_R, and it is used for tuning. The autotransformer is also used for impedance transformation to improve the performance of the Φ_2 inverter.

II. Φ_2 DC–DC Converter Design

The 13.56 MHz dc–dc converter is based on the class Φ_2 inverter in Fig. 1, followed by a resonant rectifier. In this converter, all inductors are air-cored and fabricated in part using traces on two printed circuit boards. This "printed" approach provides an improvement over previous implementations in terms of performance, ease of tuning, and reduction in component variation. In the Φ_2 inverter, C_S blocks dc and L_S sets the ac power delivered to the load R_L. Values for C_S and L_S can be selected following [1]. The remaining resonant components (L_F, L_{MR}, C_{MR}, and C_P together with MOSFET parasitic capacitance C_{OSS}) form a network that shapes the MOSFET's off-state voltage waveform to approximate a trapezoid of about $2V_{\mathrm{IN}}$ in amplitude [1], [2]. A resonant rectifier, shown in Fig. 2, is connected to the inverter and tuned to look resistive at the fundamental. The tuned rectifier

replaces R_L in the inverter of Fig. 1 and delivers dc power to constant voltage load.

The design procedure begins with the resonant rectifier. The tuning guidelines of [2] are followed throughout our design. Specifically, the value of L_R in Fig. 2 is selected to make the fundamental of $v_r(t)$ and the fundamental of $i_r(t)$ to be in phase at the rated output power and when the output voltage is kept constant at $V_{\rm OUT}$. C_R primarily consists of the diode's nonlinear junction capacitance. The number of diodes connected in parallel is chosen by ensuring that at nominal load, the average diode current is lower than the maximum rated current of each diode. As explained in [2], the rectifier tuning involves iterative simulations of the rectifier that correctly models the nonlinear behavior of the diode's junction capacitance. At nominal conditions and with the fundamental of $v_r(t)$ and $i_r(t)$ in phase, the ratio of the amplitudes of $v_{r1}(t)$ and $i_{r1}(t)$ will correspond to the resistance R_L in Fig. 1 after taking into consideration the impedance transformation gain of the autotransformer. If the ratio of the amplitudes of $v_{r1}(t)$ and $i_{r1}(t)$ is too low as to dominate the "off" MOSFET's drain–source impedance $Z_{\rm DS,off}(\omega)$ in Fig. 1, its value can be transformed with the use of an impedance matching network, a transformer or an autotransformer. The impedance transformation leads to a more efficient inverter design with larger $|Z_{\rm DS,off}(\omega)|$ and lower circulating currents. This implementation uses an autotransformer to increase the rectifier's equivalent resistance by a factor of about 4. Keep in mind that an air-core autotransformer may have significant leakage inductance. The leakage inductance can be incorporated into the design value of L_s in the inverter of Fig. 1. The modeling of the autotransformer will be detailed in Section III. Specifically, for the 400 W, 170 V input, and 28 V output converter, we parallel five CREE C3D04060E Schottky diodes whose nonlinear junction capacitance makes C_R in Fig. 2. After iterative tuning, the value of L_R that makes the rectifier behave as a resistor at the fundamental is 280 nH. Assuming the autotransformer is ideal, the impedance transformation factor is 4. The equivalent resistance of the rectifier as seen through the autotransformer is 15.7 Ω. It corresponds to the design value R_L in the inverter stage.

We continue the design by selecting values for the resonant components of the inverter stage. This begins with the selection of $C_{\rm MR}$ (with a value of tens of pF for this frequency/voltage range) that with $L_{\rm MR}$, shorts the MOSFET $Z_{\rm DS,off}(\omega)$ impedance at the second harmonic of the switching frequency f_s. The starting values of $L_{\rm MR}$ and L_F are obtained following (1) which shows an inverse relationship with $C_{\rm MR}$

$$L_F = \frac{15}{144(\pi f_s)^2 C_{\rm MR}}, \qquad L_{\rm MR} = \frac{1}{(4\pi f_s)^2 C_{\rm MR}}. \quad (1)$$

The value of $C_{\rm MR}$ is chosen to minimize the amplitude of the circulating currents at the fundamental and third harmonic of f_s. This condition is met with a low $C_{\rm MR}$ value. As $C_{\rm MR}$ is inversely proportional to $L_{\rm MR}$ and L_F, very low values of $C_{\rm MR}$ can lead to unreasonable large values of L_F and $L_{\rm MR}$ which may be impractical to implement using the air-core PCB approach.

Practically, finding final values for L_F and C_P involves iteratively obtaining the MOSFET's $Z_{\rm DS,off}(\omega)$ impedance using LTSPICE simulation. This process can be time consuming and dependent on the designer's experience. We have developed a computer script to assist in the design process with the goal of optimizing the performance of the Φ_2 inverter. The script uses Octave (A free MATLAB equivalent) [9] to write, run, and plot the results of a series of LTSPICE [10] simulations that are at the core of the iterative tuning procedure. The script labels the magnitude and phase of the MOSFET's $Z_{\rm DS,off}(\omega)$ at the fundamental second and third harmonics of the switching frequency and displays all the relevant performance metrics of the inverter (i.e., efficiency, maximum MOSFET voltage, inductor currents, etc.). Then, the script calls LaTeX to output the results in a report.

TABLE I
DESIGNED VALUES OF THE Φ_2 CONVERTER WITH $V_{\rm IN} = 170$ V AND $P_{\rm OUT} = 380$ W AT 13.56 MHZ

Part	Designed Value
MOSFET	ARF 521
diode	5*C3D04060E
C_S	3 nF
$C_{\rm MR}$	50 pF
C_P	200 pF
L_F	1000 nH
$L_{\rm MR}$	689 nH
L_S	251 nH
L_R	280 nH
autotransformer	ideal

For the converter design described here with $V_{\rm IN} = 170$ V and $P_{\rm OUT} = 380$ W, the designed values of the 13.56 MHz Φ_2 converter are listed in Table I. These values assume an ideal autotransformer with an impedance transformation factor of 4 and having no leakage inductance.

III. PCB TOROIDAL AIR-CORE INDUCTORS AND TRANSFORMERS

Electromagnetic interference (EMI) is of particular concern in air-core multimegahertz power converters. Unwanted stray magnetic fields can readily couple to near-by structures. Early implementations of Φ_2 dc–dc converters used solenoidal inductors to simplify fabrication at the expense of increased EMI [1], [11]. The use of toroidal air-core inductors addresses some of these issues, by constraining the magnetic field to the torus. But stray magnetic fields remain due to the suboptimal copper coverage of the structure. Better inductors have been studied in [12], which have lower losses at high frequency and better repeatability, but are challenging to fabricate. The authors in[13] and [14] study the toroids that use the opposite layers of the same PCB and vias to close turns. This limits inductor size, making it difficult to obtain larger value inductors.

The inductors and autotransformer used here are designed for a high Q and easily implemented using traces and copper planes on two PCBs separated by constant length copper filaments to close the turns of the toroids. This is a simple way to obtain a stable, repeatable, and self-shielded magnetic structure to use in the converter described here. Compared to wire-wound toroidal

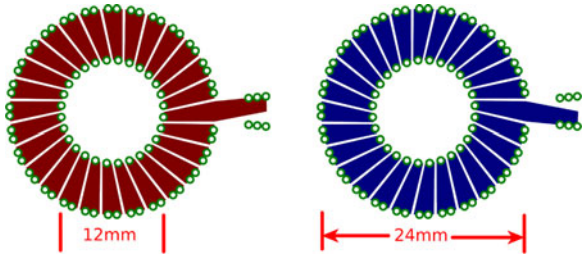

Fig. 3. Layout of L_F, a 28-turn PCB inductor used in the converter describe here: The figure shows the bottom part (blue) and top part (red) of the toroid that is placed in two aligned but separate PCBs. Here, the inner diameter is 12 mm, and the outer diameter is 24 mm; drill diameter of the vias is 0.6 mm; minimum separation between turns is 0.38 mm.

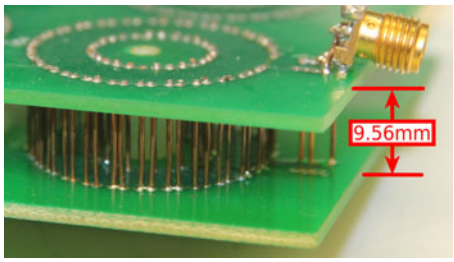

Fig. 4. Side view of the 28-turn PCB inductor L_F introduced in Fig. 3: The measured inductance is 1071 nH when the two parts of the toroid are maintained 9.56 mm apart using vertical copper wires.

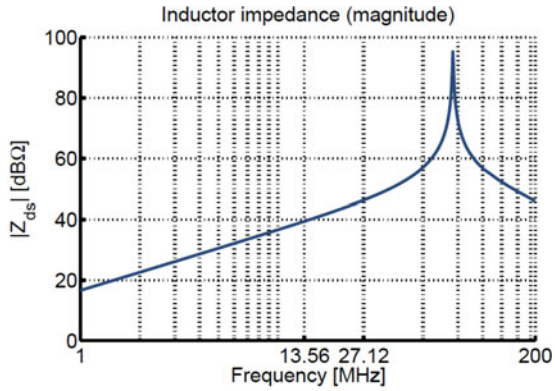

Fig. 5. Measured impedance (magnitude) of the inductor of L_F shown in Fig. 3 and 4: Notice the self-resonance around 76.6 MHz. This is due to the interwinding capacitance of the structure.

Fig. 6. Wire-wound counterpart inductor for comparison with the PCB inductor in Fig. 4. The dimensions are listed in Table III.

inductors especially with small number of turns, PCB inductors utilize the space between turns more efficiently and, therefore, can achieve higher quality factors.

A. *Example Inductor Implementation*

Fig. 3 shows the PCB traces that form the inductor L_F of our design. It is a 28-turn air-core toroidal inductor laid out in Eagle [15] using an Octave script. In this script, the designer enters the number of turns, the inner and outer diameters of the toroid, the diameter of the vias that will link the two boards, the minimum trace separation, and few other parameters. Upon execution, the Octave script writes an Eagle ".scr" file with the geometric description of the air-core toroid. The resulting PCB layout and the traces in their corresponding layers are stored in a component library available for PCB layout of the converter. Fig. 4 shows the side view implementation of the inductor L_F. The two PCBs are separated by 9.56 mm using vertical copper wires. The wires used to close the inductor turns is 0.511 mm in diameter. As an initial proof of concept, we placed a nylon board spacer at the center of each toroidal structure to help maintain a constant separation between the top and bottom PCB boards. The spacers were left in place adding to the structural stability of the converter. The individual wires closing the inductor turns connecting the top and bottom boards are soldered which also adds to mechanical stability. As the inductor quality factor increases with height, we are interested in having reasonable toroid heights while maintaining mechanically stability. In a later implementation of the two board technique [16], the PCB inductors were implemented using a single 3.2 mm PCB (standard PCBs are 1.6 mm from most PCB inexpensive manufacturers) for a 27.12 MHz converter. A single board design greatly reduces mechanical instabilities. The inductor values needed for the 13.56 MHz design presented here, specially the autotransformer described below, could not be implemented on a single board. Eventually, we want all passive resonant components to be embedded in the internal layers of a PCB multilayer structure. This will greatly reduce tuning complexity.

In order to ensure the values of these PCB inductors correspond to the designed values, the inductors are first implemented and measured individually. An Agilent E5061B impedance analyzer is used to measure the impedance of each PCB inductor in the 1–200 MHz range. Fig. 5 shows the impedance of one PCB inductor L_F used in the converter. The inductor shows a parallel self-resonance at 76.6 MHz. This is at a frequency which is higher than the relevant frequencies of the design and has little effect on the converter performance. The parallel resonance is dominated by the interwinding capacitance resulting from the proximity and thickness of the copper filaments closing the toroid turns. In order to show the benefits of implementing resonant toroids with PCB traces to reduce inductance variation, we constructed and measured two additional PCB inductors of the same dimensions. Moreover, three wire-wound air-core inductors were also built and measured for comparison. Fig. 6 shows one of the wire-wound inductors for this comparison. Table III lists the dimensions and the measured inductance. It is clear that inductance variation of the wire-wound inductors can reach up

TABLE II
PCB INDUCTORS SPECIFICATIONS

	d_i/d_o/Ht [mm]	Turns	Calc [nH]	Meas [nH]	Q calc @f_s	Q mea @f_s
L_F	12/24/9.56	28	1052	1071	207	160
L_{MR}	11/22/9.56	23	713	750	189	123
L_S	8/16/9.56	7	74	84	155	90

The measured values include the inevitable extra inductance added when placing SMA connectors used during impedance measurements (see Fig. 4).

TABLE III
COMPARISON IN INDUCTANCE VARIATION BETWEEN A SET OF PCB INDUCTORS AND A SET OF HAND WOUND AIR-CORE INDUCTORS

	d_i/d_o/Ht [mm]	Turns [nH]	Meas [nH]
PCB 1	12/24/9.56	28	1071
PCB 2	12/24/9.56	28	1070
PCB 3	12/24/9.56	28	1080
Wire 1	13/25.12/9.56	28	1517
Wire 2	13/25.12/9.56	28	1596
Wire 3	13/25.12/9.56	28	1581

The maximum inductance variation in the PCB inductors is of $\approx 1\%$ of the minimum inductance value. For the tested hand wound wire inductors, this difference is of$\approx 5\%$.

to 5%, while the PCB inductors shows a variation of $\approx 1\%$. Part of the inductance variation in the wire inductors is because these were wound by hand, and lower variation in inductance values is expected in machine wound toroids. However, this is also true of the PCB inductors, and it is likely that very tight tolerances on inductor values are achievable with the latter. A thorough study of inductance variations on machine fabricated parts is outside the scope of this paper.

Table II provides details of the PCB inductors used in the converter including the dimensions, the measured inductance values and Q, and the estimated inductance values following (2) provided in [12]. The first term on the right-hand side of (2) represents the inductance induced by the flux inside the toroid, while the second term represents the inductance of the single-turn loop around the center of the toroid

$$L = \frac{N^2 h \mu_0}{2\pi} ln\left(\frac{d_o}{d_i}\right) + \frac{d_i + d_o}{4}\mu_0\left[ln\left(8\frac{d_o + d_i}{d_o - d_i}\right) - 2\right]. \quad (2)$$

The PCB toroid dimensions were chosen to meet a target inductance value, under the constraint that all inductors were of the same height. This made the process of assembling the converter simpler. We then tried to minimize component area, but limitations in size, spacing, and clearance of traces and vias, constrain the design space of our components. Specifically, we were limited by the minimum diameter a toroid could have given that each segment of the toroids needs at least one via to complete the inductor turn, separated from other vias by the minimum clearance specified by the board manufacturer. Tradeoffs in size, inductance value, and quality factor resulted in the dimensions of the three PCB inductors used in the final implementation. The same constraints apply to PCB autotransformer discussed below.

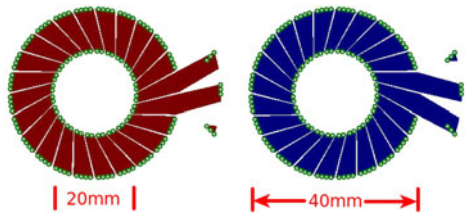

Fig. 7. Layout of the 24-turn PCB autotransformer: The wedges on the 12-turn primary winding are intercalated with the 12-turn secondary. Both windings are then connected as an autotransformer. The figure shows the top section (red) and bottom section (blue). The inner diameter of the structure is 20 mm, while the outer diameter is 40 mm. The minimum separation between turns is 0.58 mm.

For inductance values, the measured values include the extra inductance added between the leads of the inductor and the SMA connectors used during impedance measurements. The impedance analyzer calibration process includes the effect of the SMA connectors themselves. This can contribute to the discrepancy between the measured values and calculated values, along with other factors such as stray capacitance. The value of L_S listed in Table II differs very significantly from the design value listed in Table I because this new value reflects the impact of the leakage inductance of the autotransformer. The autotransformer leakage inductance appears in series with L_S and C_S as described in the following section.

Even though the PCB inductor presented here has a repeatable structure and smaller inductance variation is expected, there still exists variations due to the copper wire passing process. Future work will improve the PCB inductor implementation by reducing or eliminating the copper wire passing process. Also, another part will be to evaluate the tradeoffs in the design of PCB inductors to improve performance while increasing the parallel self-resonant frequency.

B. Autotransformer

Similar to the design of the air-core inductors, a PCB autotransformer is generated using an Octave script incorporating minor changes to the geometry of the structure. Specifically, the autotransformer is constructed by properly connecting the windings of a 1:1 air-core toroidal transformer simply formed by alternating turns in a PCB toroidal structure. The top and bottom traces forming the sections of a 24-turn autotransformer are shown in Fig. 7. Fig. 8 shows a side-view picture of the autotransformer having 20 mm inner diameter and 40 mm outer diameter. The length of the filaments closing the turns of the winding is the same as the inductors (9.56 mm).

Remember that the autotransformer performs multiple functions: 1) resonant inductance of the rectifier; 2) impedance transformation; and 3) contributes to L_S. When connected as an autotransformer, it increases the equivalent resistance of the rectifier by a factor of approximately 4. The autotransformer is modeled and characterized using the cantilever model and parameter extraction methods of in [17] (Cantilever equivalent

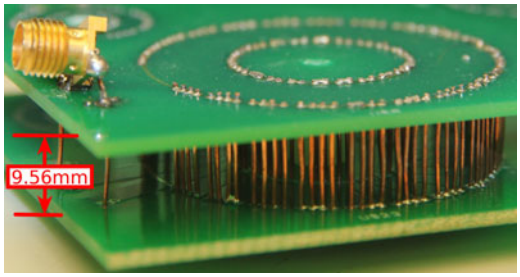

Fig. 8. Side view of the 24-turn PCB autotransformer used in the converter: Vertical separation is 9.56 mm.

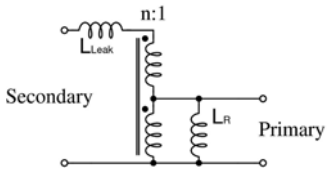

Fig. 9. Autotransformer cantilever model.

TABLE IV
PCB AUTOTRANSFORMER SPECIFICATIONS

Model Part	Measured Value	Description
L_R	260 nH	Q=120
L_{Leak}	171 nH	Q=52
n	1.82	effective turns ratio

model shown in Fig. 9). We then extract the electrical parameters including the effective autotransformer ratio n, magnetizing inductance L_R, and leakage inductance L_{Leak}. The extracted autotransformer parameters are listed in Table IV at the switching frequency.

IV. GATE DRIVE IMPLEMENTATION

In converters operating above 10 MHz frequencies, gate drive circuit design presents a challenge [2]. Hard switching drives have been assumed prohibitively lossy; hence, several resonant strategies have been devised that efficiently drive the transistor gate in switching converters up to 110 MHz [18], [19]. A sinusoidal scheme [20] is efficient and simple but makes timing control difficult. Moreover, the gradual transitions of a sine wave increase loss in the power stage. This results from a decreasing drive at the end of the on-interval, where high drain current exacerbates losses. The trapezoidal gate drive of [2] and [21] uses the Φ_2 network to reduce conduction losses but this approach increases tuning complexity.

A 13.56 MHz hard-switched gate drive is used in this design. A simplified schematic of the gate drive used here is shown in Fig. 10. The circuit is divided into three functional parts: a clock signal generator, control of the pulse length, and a high current MOSFET gate drive integrated circuit. The clock signal generation is made of an oscillator and an enable signal which can modulate the gate drive for potential ON–OFF control scheme.

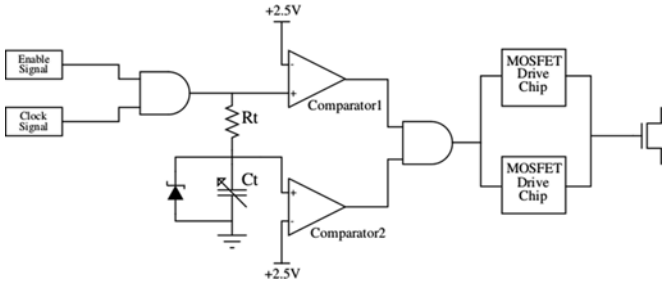

Fig. 10. Simplified gate drive schematic.

TABLE V
COMPONENTS IN GATE DRIVE BOARD

Quantity	Mft. Part No.	Description
1	CCR27.12MYC7B05T1	27.12-MHz ceramic resonator
1	74AHC1G79GW.125	D-flip flop
2	SN74LVC2G04DBVR	inverter
2	NC7SZ08M5X	AND gate
1	LT1720CMS8PBF	dual comparator
1	CRCW0805430RFKEA	R_t
1	SGC3S300	C_t
1	BAT54-TP	zener diode
2	ISL55110IRZ	MOSFET Driver Chip
15	GRM21BR71H104KA01L	0.1-μF bypass capacitors
2	TAJB335K035RNJ	3.3-μF bypass capacitor

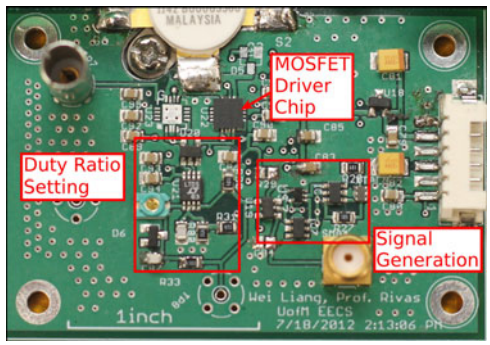

Fig. 11. Gate drive board.

The gate pulsewidth is controlled with the dual comparator and resistor–capacitor–divider network. If a single gate driver is insufficient, two MOSFET gate drives can be paralleled to provide enough power for the MOSFET. The components forming the gate drive are listed in Table V. Fig. 11 shows the circuit implementation. Great care and good layout practices are observed during the layout of the gate drive board to minimize parasitic inductances that could lead to undesirable ringing. Fig. 12 shows the gate voltage during the converter operation. To minimize ringing of the gate signal, thin traces need to be avoided at the MOSFET gate terminal to minimize the parasitic inductance. Also for proper cooling, additional vias underneath the Intersil ISL55110 chip are important to dissipate heat.

We have taken into consideration the tradeoffs between simplicity and power loss of this hard-switched gate drive at 13.56 MHz frequency. Compared to the aforementioned res-

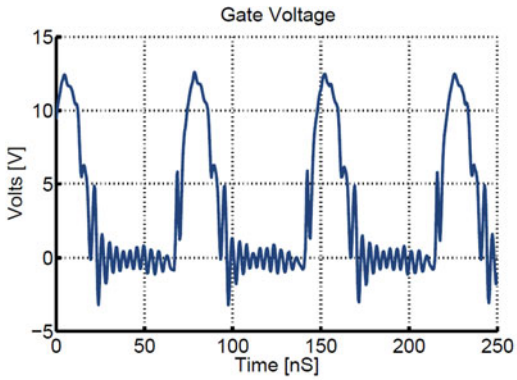

Fig. 12. Measured gate voltage: Measured power loss is about 2.35 W with an input voltage 10 V.

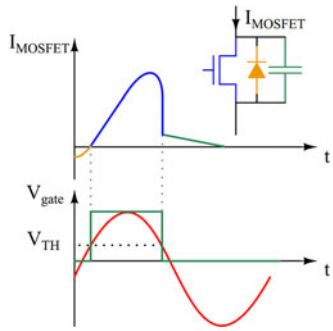

Fig. 13. Comparison between square wave hard-switched gate drive and sinusoidal resonant gate drive. The square wave gate drive applies a larger gate voltage while the MOSFET current is high, which reduces the $R_{\mathrm{ds,ON}}$ value and conduction losses.

onant gate drive schemes, the hard-switched gate drive does not need the auxiliary switch or additional resonant stage. In addition to its simplicity, this driver reduces conduction losses of the circuit by applying a larger gate voltage driving the MOSFET as shown in Fig. 13, which mitigates the additional gate drive losses. The gate drive dc input power is about 2.35 W including $C_g v_{gs}^2 f_s$ loss. It is about 1.2–0.5% of the output power of the converter (200–400 W).

V. Experimental Verification

A. Converter With PCB Inductors

The MOSFET used in our design is the Microsemi ARF521. It has a 500 V breakdown voltage and about 1 Ω R_{dson} at operating temperature. The rectifier diode is implemented by paralleling five SiC CREE C3D04060E Schottky diodes. Each has a breakdown voltage of 600 V and about 2 V forward voltage drop. The positive temperature characteristics make parallel combination possible to handle a large current. Table VI shows the components used in this prototype.

Careful considerations are followed through the layout of the converter. Particularly, we avoid placing large ground planes in the bottom layer of the board in places that could result in large parasitic capacitance with the potential to adversely affect the impedance of the design. Significant effort is also made in trying to minimize unnecessary parasitic inductances wherever appropriate.

TABLE VI
Components in Converter With PCB Inductors

Part	Measured Value	Part No. and Description
MOSFET	ARF 521	RF Power MOSFET
diode	5*C3D04060E	CREE SiC Schottky diode
C_{IN}	3 μF	3*GRM55DR72E105KW01L
C_{OUT}	0.6 μF	6*VJ1825Y104KXCAT
C_S	3 nF	2*MC22FF152J-F
C_{MR}	46 pF	6*ATC700B
C_P	200 pF	2*ATC700B
L_F	1071 nH	PCB inductor
L_{MR}	750 nH	PCB inductor
L_S	90 nH	PCB inductor
Autotransformer	260 nH/171 nH/1.82	PCB autotransformer

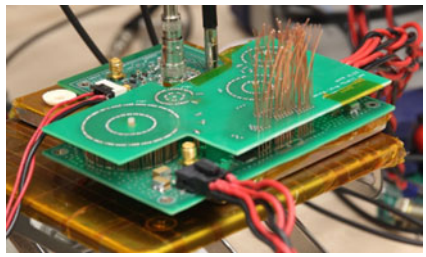

Fig. 14. Converter with PCB inductors: Diodes, input, and output capacitors are covered by the upper board.

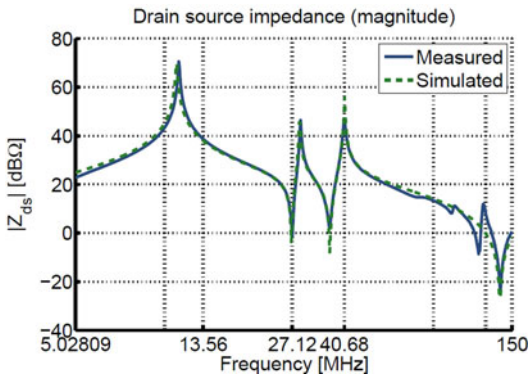

Fig. 15. Drain impedance measurement versus simulation of converter with PCB inductors.

Impedance measurement at MOSFET drain node is important to verify the components' on board values and capture parasitics. Once the MOSFET and diodes are soldered to the board, the measurement is taken under biased condition with an input voltage of 170 V and output voltage of 28 V. Fig. 14 shows the converter with PCB inductors after implementation. Fig. 15 shows the drain impedance comparison between simulation and experimental results. Our measurement setup is shown in Fig. 16. Input and output voltages are measured using banana hooks on the board directly. Input and output currents are converted through Agilent 34330A current shunts to voltages. MOSFET drain voltage and diode anode voltage are monitored.

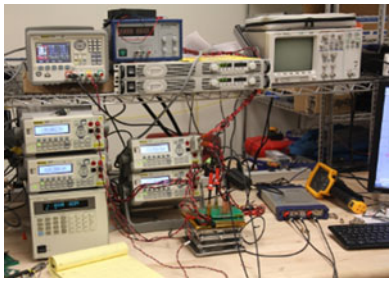

Fig. 16. Measurement setup including two Agilent N5700 power supplies in parallel as the main power supply, one Rigol DP1308A power supply to power the gate drive circuit, one Agilent N3301A electronic load as the constant voltage load, four Rigol DM3068 digital multimeters and Picoscope 6000 series USB oscilloscope.

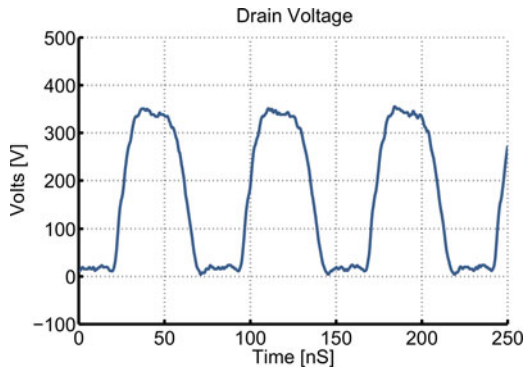

Fig. 17. Measured drain voltage of converter with PCB inductors.

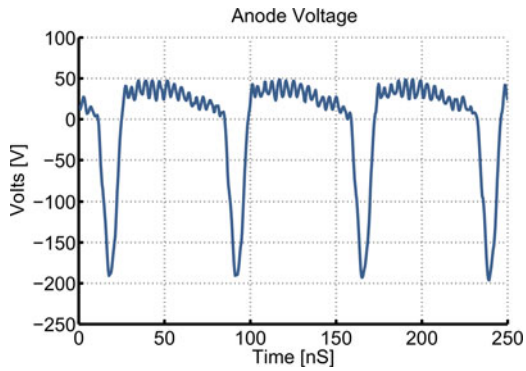

Fig. 18. Measured anode voltage of converter with PCB inductors.

Figs. 17 and 18 show the drain and anode voltage experimental waveforms, respectively.

Power and efficiency measurements are performed with different input voltages. Fig. 19 displays the output power and efficiency as the input voltage varying from 160 to 180 V. At the nominal input voltage 170 V, the converter outputs 313 W and has an efficiency of 77% including the gate drive power. A simulated loss breakdown is provided in the Table VII. About 60% of the total loss is mainly due to conduction losses in the semiconductor devices (MOSFET and diodes). Because soft switching is implemented, switching losses are negligible. The power density of this particular design reaches about 80 W/in^3. Optimization for better efficiency, miniaturization, and EMI shielding of the converter with PCB inductors has not been fully studied. It remains a direction for our future work.

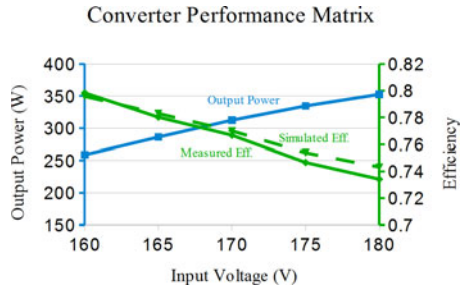

Fig. 19. Metrics of converter with PCB inductors, output power (blue line), measured efficiency (green solid line), and simulated efficiency (green dash line).

TABLE VII
SIMULATED LOSS BREAKDOWN AT THE NOMINAL OPERATING POINT

	% Loss
MOSFET	38.1
Diode	22.5
AutoXf	30.5
L_F	1.8
L_{MR}	4.7
L_S	1.1
Others	1.3

A large fraction of the losses in the converter is due to conduction in the Si MOSFET. The number of MOSFETs available, having the proper rating and in a low inductance package suitable for our design, are very low, a situation that to a certain extent constrained our maximum efficiency. The overall efficiency was not as good as anticipated as losses in the autotransformer were somewhat higher than expected. As a comparison in performance, work in [2] first presents the Φ_2 dc–dc converter. The converter switches at 30 MHz and has the output voltage 33 V. The efficiency reaches 82.5% at $V_{\mathrm{IN}} = 200$ V and $P_{\mathrm{OUT}} = 300$ W. Work in [22] presents a 900 W 30 MHz Φ_2 converter. The efficiency is 79%. Work in [11] presents a 30 MHz 500 W Φ_2 push–pull converter with 80% efficiency.

Work in [23] predicts the power density of the pulse width modulation power converters for automotive applications will reach between 80 and 160 W/in^3 by 2020. And automotive is one area that this converter can contribute greatly. This in our view makes the 80 W/in^3 achieved by this converter acceptable. Moreover, as we optimize our design procedure, we expect further gains in power density.

It is difficult to draw power density comparisons between this converter and others in which the PCB embedded inductors were implemented using magnetic material, like the work in [24], as the area application and output voltages are very different. But we think air-core inductors have the potential to shrink in size further as the switching frequency increases, and we optimize the number/size of vias. For example, a lower power design we later presented in [16] used a 86-nH inductor implemented us-

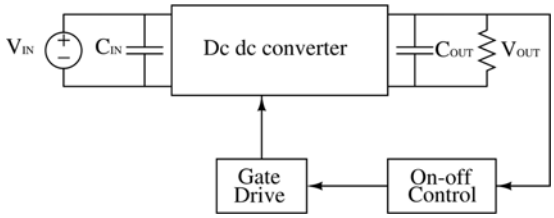

Fig. 20. Schematic of the control scheme.

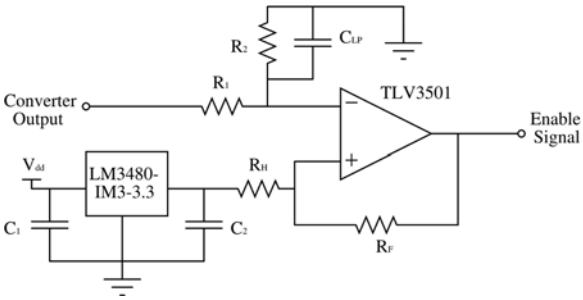

Fig. 21. Hysteresis controller used in the ON–OFF control scheme.

TABLE VIII
CONTROLLER PARAMETERS

Parameter	Value	Units
R_1	25	kΩ
R_2	3.3	kΩ
R_H	1	kΩ
R_F	220	kΩ
C_1	0.6	μF
C_2	0.1	μF

ing a single 3.2-mm PCB for 27.12-MHz operation. Moreover, by not having magnetic material, the air-core inductors may be able to operate at higher temperature, if implemented on a high-temperature laminate (PTFE). Also, applications in strong magnetic fields are possible (MRI) without compromising the performance of inductor. Further optimization to improve converter efficiency or improve EMI shielding of a converter using PCB inductors has not been fully studied yet. It remains a direction in our continuous work in this area.

B. Closed-Loop Control of Converter With PCB Inductors

An ON–OFF control scheme is applied to the converter with PCB inductors to regulate the output voltage. As shown in the Fig. 20, the ON–OFF controller senses the output voltage and sends enable signals to the gate drive circuit. Therefore, the power stage is switched ON and OFF at a frequency lower than the switching frequency [2]. A simple way to implement the ON–OFF controller is to use a hysteresis controller. The schematic is shown in Fig. 21, and values are listed in Table VIII. In addition, a proper output capacitance value is selected to control the converter modulation frequency. In our design, the output capacitance is 119 μF.

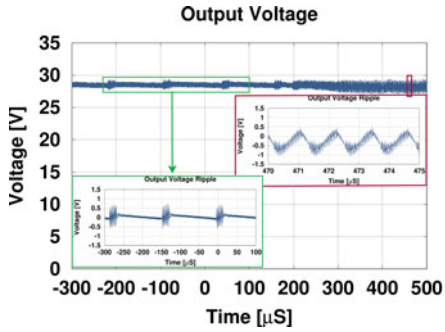

Fig. 22. Output voltage as the load step changed from 100 Ω ($P_{\rm OUT}$ = 8 W) to 4.76 Ω ($P_{\rm OUT}$ = 168 W) at t = 200 μs. The waveform is filtered at 150 MHz. The left inserted figure shows the voltage ripple for 100 Ω load, while the right inserted figure shows the 4.76 Ω.

When the converter is under ON–OFF control, efficiency is penalized due to the transition between ON and OFF periods. In this case, the efficiency comes down to 71.9%, when the converter is connected to a 4.76 Ω (a 5 Ω in parallel with a 100 Ω) resistance load.

The converter system is also tested under a load step change in order to demonstrate the transient response. The load resistance consists of a 5 Ω and a 100 Ω power resistor in parallel. In order to trigger a fast resistance change, a MOSFET (Fairchild FQP30N06L) is connected in series with the 5 Ω resistor [2]. Fig. 22 displays the waveform of the converter output voltage ripple as the load changes from 100 to 4.76 Ω at time 200 μS. As expected, the transient time of the output voltage ripple is as short as microseconds due to the low energy stored in the converter.

C. Repeatability of the Converter With PCB Inductors

In order to prove the repeatability of the converter implementation, we ask another student to replicate the converter with PCB inductors using the same components as the original one. To be rigorous, the student has no knowledge of the tuning procedure before he implemented the replicate converter. Also, no intermediate measurement is taken to capture the parasitics on purpose during this replication process. When the implementation is completed, the drain node impedance is measured with the input and output biased at the nominal voltages. Fig. 23 together with Fig. 15 show the close agreement between simulation and measured impedance as well as between the original converter and replicate converter.

The replicate converter is measured under the same conditions as the original one. Figs. 24 and 25 display the MOSFET drain voltage and diode anode voltage, respectively. The replicate converter yields 309 W with an efficiency of 76.3%.

Both the impedance and performance measurement of the replicate converter prove the repeatability of the implementation process of the converter with PCB inductors. The requirement of the converter tuning procedure knowledge is reduced to minimum during the implementation process, while the converter performance remains the same.

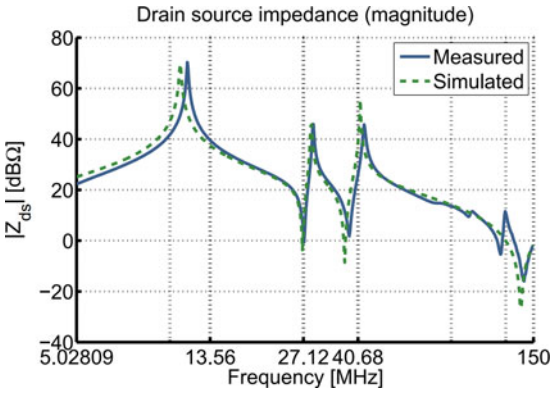

Fig. 23. Drain impedance measurement versus simulation of the replicate converter.

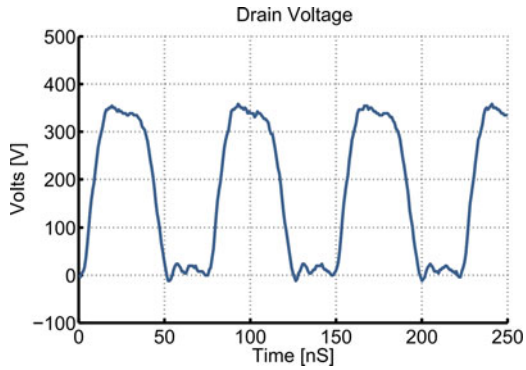

Fig. 24. Drain voltage of the replicate converter.

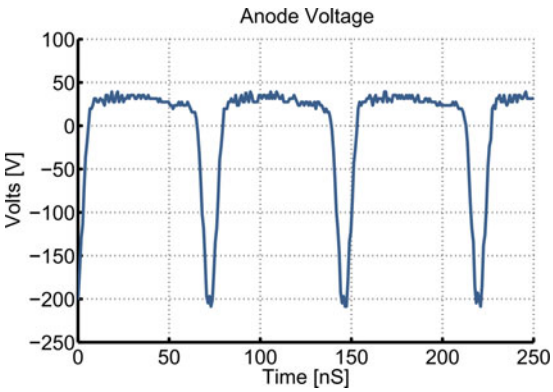

Fig. 25. Anode voltage of the replicate converter.

TABLE IX
COMPONENTS IN CONVERTER WITH WIRE-WOUND INDUCTORS

Part	Measured Value	Part No. and Description
MOSFET	ARF 521	RF Power MOSFET
diode	5*C3D04060E	CREE SiC Schottky diode
C_{IN}	1.4 μF	14*VJ1825Y104KXEAT
C_{OUT}	0.7 μF	7*VJ1825Y104KXCAT
C_S	6 nF	4*MC22FF152J-F
C_{MR}	71.6 pF	6*ATC700B
C_P	200 pF	2*ATC700B
L_F	623 nH	27-turn AWG 16
L_{MR}	471 nH	24-turn AWG 16
L_S	162 nH	12-turn double AWG 16
Autotransformer	263 nH/121 nH/1.88	32-turn AWG 16
Coil form	T80-0	Micrometal, Inc.

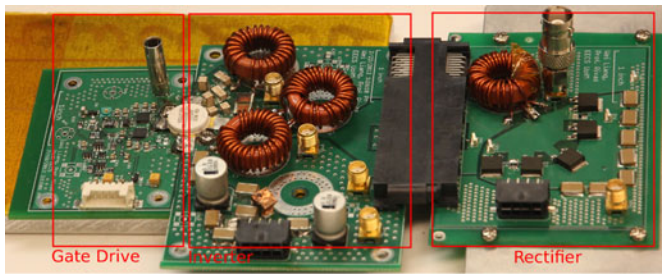

Fig. 26. Converter with wire-wound inductors.

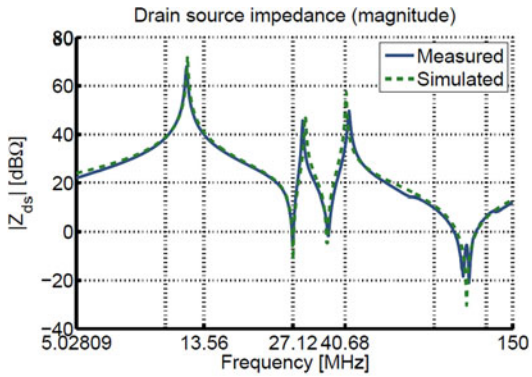

Fig. 27. Drain impedance measurement versus simulation of converter with wire-wound inductors.

D. Converter With Wire-Wound Inductors

This converter uses the same semiconductors and capacitor types but a different way to implement inductors. Three inductors are implemented using magnet wires wound on toroidal plastic coil forms. Table IX displays the components used in this converter.

Compared to PCB inductors, these inductors are more sensitive to variation. Inductance values can change 5% to 10% of their off-board measured values by touching and slight tweak during the soldering process. In order to account for such changes and other parasitics, it is necessary to verify the MOSFET drain impedance step by step after each component is soldered. This implementation and verification process is highly dependent on designer's experience and can be very time consuming. For this converter, we are able to capture the impedance characteristics by matching the measured drain impedance and simulation. Fig. 26 shows the converter prototype, and Fig. 27 shows the comparison between simulation and experimental results.

Using the same setup as mentioned above, the drain and anode waveforms are monitored. Figs. 28 and 29 show the drain and anode voltage experimental waveforms, respectively.

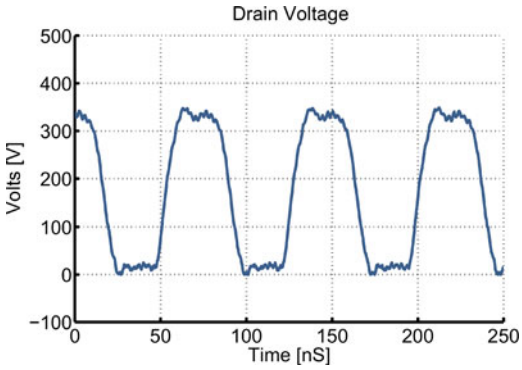

Fig. 28. Measured drain voltage of converter with wire-wound inductors.

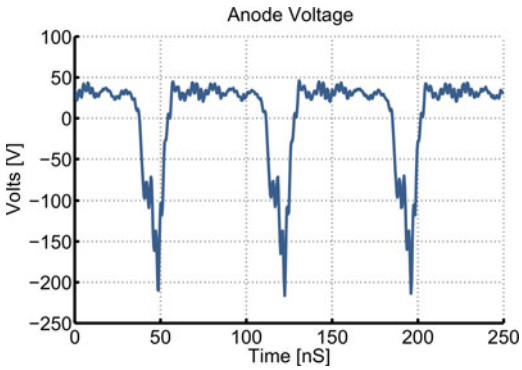

Fig. 29. Measured anode voltage of converter with wire-wound inductors.

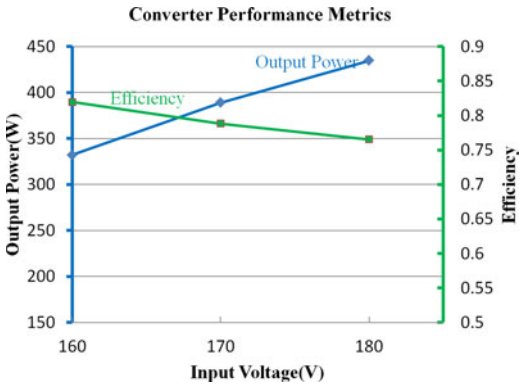

Fig. 30. Metrics of converter with wire-wound inductors.

Power and efficiency measurements are performed with different input voltages. Fig. 30 displays the output power and efficiency as the input voltage varying from 160 to 180 V with a 10 V step. At the nominal input voltage of 170 V, the converter outputs 388 W and has an efficiency of 77% including the gate drive losses. A simulated loss breakdown is provided in the Table X.

Over 60% of the total loss is mainly due to the semiconductor conduction loss since the soft switching operation of the semiconductors. The power density of this converter is about 60 W/in^3.

TABLE X
SIMULATED LOSS BREAKDOWN

	% Loss
MOSFET	47.8
Diode	21.4
AutoXf	21.1
L_F	1.7
L_{MR}	1.9
L_S	1.6
Others	4.5

VI. CONCLUSION

This paper presents the design and implementation of a high density 150–200 V to 28 V, 200–400 W Φ_2 dc–dc converter with PCB inductors. The converter has a switching frequency of 13.56 MHz and uses air-core toroidal inductors formed as part of the PCB. The PCB inductors reduce inductance variation, minimize unwanted stray magnetic fields, and reduce uncertainty in parasitics and undesired coupling to the rest of the circuit. Hence, the tuning and implementation of the converter are simplified while achieving high levels of performance and power density. In the near future, optimization of the PCB inductors, the study of the EMI, and the other integration process will be done to pursue higher power density and performance level.

ACKNOWLEDGMENT

The authors would like to thank L. Raymond and F. Lu's generous help throughout the experiments and the paper editing.

REFERENCES

[1] J. M. Rivas, Y. Han, O. Leitermann, A. Sagneri, and D. J. Perreault, "A high-frequency resonant inverter topology with low voltage stress," in *Proc. IEEE Power Electron. Spec. Conf.*, 2007, pp. 2705–2717.

[2] J. M. Rivas, O. Leitermann, Y. Han, and D. J. Perreault, "A very high frequency dc–dc converter based on a class Φ_2 resonant inverter" *IEEE Trans. Power Electron.*, vol. 26, no. 10, pp. 2980–2992, Oct. 2011.

[3] N. Sokal and A. Sokal, "Class E-a new class of high-efficiency tuned single-ended switching power amplifiers," *IEEE J. Solid-State Circuits*, vol. SSC-10, no. 3, pp. 168–176, Jun. 1975.

[4] R. Redl and N. Sokal, "A 14 MHz 100 Watt class E resonant converter: Principles, designconsiderations, and measured performance," in *Proc. 17th Annu. IEEE Power Electron. Spec. Conf. Proceed.*, pp. 69–77, 1986.

[5] R. Redl, B. Molnar, and N. Sokal, "Class E resonant regulated dc/dc power converters: Analysis of operations and experimental results at 1.5 MHz," *IEEE Trans. Power Electron.*, vol. PE-1 no. 2, pp. 111–120, Apr. 1986.

[6] R. Redl and N. Sokal, "A new class-E dc/dc converter family with reduced parts count: Derivation, topologies and design considerations," in *Proc. Techn. Papers 4th Int. High Freq. Power Conf.*, pp. 395–415, 1989.

[7] J. Jozwik and M. Kazimierczuk, "Analysis and design of class E^2 dc/dc converter," *IEEE Trans. Ind. Electron.*, vol. 37, no. 2, pp. 173–183, Apr. 1990

[8] H. Koizumi, M. Iwadare, and S. Mori, "Class E^2 dc-dc converter with second harmonic resonant class E inverter and class E rectifier," in *Proc. 3rd Annu. Appl. Power Electron. Conf. Proceed.*, 1994, pp. 1012–1018.

[9] GNU Octave. Computer Software. (2013). [Online]. Available: http://www.gnu.org/software/octave/index.html

[10] L. Technology. LTspice IV. Computer Software. (2014). [Online]. Available: http://www.linear.com/designtools/software/

[11] J. S. Glaser and J. M. Rivas, "A 500 W push-pull dc-dc power converter with a 30 MHz switching frequency," in *Proc. 25th Annu. IEEE Appl. Power Electron. Conf. Expo.*, 2010, pp. 654–661.

[12] C. R. Sullivan, W. Li, S. Prabhakaran, and S. Lu, "Design and fabrication of low-loss toroidal air-core inductors," in *Proc. IEEE Power Electron. Spec. Conf.*, 2007, pp. 1754–1759.
[13] S. Orlandi, B. Allongue, G. Blanchot, S. Buso, F. Faccio, C. Fuentes, M. Kayal, S. Michelis, and G. Spiazzi, "Optimization of sheilded PCB air-core toroids for high efficiency dc-dc converters," *IEEE Trans. Power Electron.*, vol. 26, no. 7, pp. 1837–1846, Jul. 2011
[14] M. Ludwig, M. Duffy, T. O'Donnell, P. McCloskey, and S. Mathuna, "PCB integrated inductors for low power dc/dc converter," *IEEE Trans. Power Electronics*, vol. 18, no. 4, pp. 937–945, Jul. 2003.
[15] C. C. GmbH and C. Inc. EAGLE PCB Software. Computer Software. (2014). [Online]. Available: http://www.cadsoftusa.com/?language=en
[16] L. Raymond, W. Liang, J. Choi, and J. Rivas, "27.12 MHz large voltage gain resonant converter with low voltage stress," in *Proc. IEEE Energy Convers. Congr. Expo.*, 2013, pp. 1814–1821.
[17] R. Erickson and D. Maksimovic, "A multiple-winding magnetics model having directly measurable parameters," in *Proc. IEEE Power Electron. Spec. Conf.*, 1998, pp. 1472–1478.
[18] Y. Han, O. Leitermann, D. A. Jackson, J. M. Rivas, and D. J. Perreault, "Resistance compression networks for radio-frequency power conversion," vol. 22, no. 1, pp. 41–53, 2007.
[19] R. Pilawa-Podgurski, A. D. Sagneri, J. M. Rivas, D. I. Anderson, and D. J. Perreault, "Very-high-frequency resonant boost converters," vol. 24, no. 6, pp. 1654–1665, 2009.
[20] J. M. Rivas, "*Radio frequency dc-dc power conversion*," Ph.D. dissertation, *Elect. Eng. Comput. Sci.*, Massachusetts Inst. Technol., Cambridge, MA, USA, 2006.
[21] B. Song, X. Yang, and Y. He, "Class Φ_2 dc-dc converter with PWM on-off control," in *Proc. IEEE 8th Int. Conf. Power Electron. EECE Asia*, pp. 2792–2796, 2011.
[22] J. S. Glaser, J. Nasadoski, and R. Heinrich, "A 900 W, 300 V to 50 V dc-dc power converter with a 30 MHz switching frequency," in *Proc. 24th Annu. IEEE Appl. Power Electron. Conf. Expo.*, 2009, pp. 1121–1128.
[23] J. Kolar, U. Drofenik, J. Biela, M. Heldwein, H. Ertl, T. Friedli, and S. Round, "PWM converter power density barriers," in *Proc. IEEE Power Convers. Conf*, Nagoya, Japan, 2007, pp. P-9–P-29.
[24] Y. Su, W. Zhang, Q. Li, F. Lee, and M. Mu, "High frequency integrated point of load (POL) module with PCB embedded inductor substrate," in *Proc. IEEE Energy Convers. Congr. Expo.*, 2013, pp. 1243–1250.

Wei Liang (S'12) received the B.Eng. degree from Northwestern Polytechnical University, Xi'an, China, and the M.S.E. degree from the University of Michigan, Ann Arbor, MI, USA, in 2011 and 2013, respectively. He is currently working toward the Ph.D. degree at the Stanford University Power Electronics Research Laboratory, Stanford University, Stanford, CA, USA.

His research interests include power electronics and the air-core passive components design for VHF power conversion.

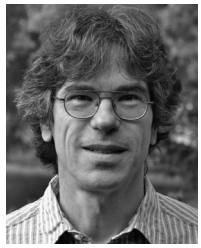

John Glaser (SM'10) received the B.S.E.E. degree from the University of Illinois, Urbana-Champaign, Champaign, IL, USA, and the M.S.E.E. and Ph.D. degrees in electrical engineering from the University of Arizona, Phoenix, AZ, USA, in 1987, 1991, and 1996, respectively.

He has worked on mobile RF power amplifiers for Motorola and on high-voltage dc–dc converters for TWT amplifiers for Hughes Missile Systems Co. From 1998 to 2014, he was at General Electric Global Research in Niskayuna, NY, USA, serving both technical and project leadership roles. Projects at GE included high-performance dc–dc and ac–dc converters, VHF amplifiers, induction heating, electronic ballasts, and magnetics for power electronics, for applications ranging from lamp drivers to MRI. In 2014, he served as the Director of Applications Engineering at Efficient Power Conversion Corporation, where his role is to develop applications, circuits, and methods to maximize the benefit of gallium nitride power transistors and to drive adoption in the power electronics community. His current research interests include high-efficiency VHF power processing and wide bandgap (silicon carbide and gallium nitride) power device testing, modeling and application. He has published more than 20 papers in the area of power electronics and has been granted 25 U.S. patents, with several more pending.

Juan Rivas (S'01–M'06) was born in Mexico City, Mexico. He received the B.A.Sc. degree from the Monterrey Institute of Technology, Monterrey, Mexico, in 1998, and the S.M. and Sc.D. degrees from the Laboratory of Electromagnetic and Electronic Systems, Massachusetts Institute of Technology, Cambridge, MA, USA, in 2003 and 2006, respectively.

From 2007 to 2011, he was a Power Electronics Engineer in the high-frequency power electronics group at the General Electric Global Research Center, Niskayuna NY, USA. From 2011 to 2013, he was an Assistant Professor at the University of Michigan, Ann Arbor, MI, USA. In 2014, he joined Stanford University, Stanford, CA, USA, as an Assistant Professor in the Electrical Engineering Department. His research interests include power electronics, RF power amplifiers, resonant converters, soft switching topologies, and the design of air-core passive components for VHF power conversion.